Acta Mineralogica-Petrographica, Szeged 2002, Vol. 43, pp. 27-38

ACTA
Mineralogica
Petrographica

ORIGIN AND TECTONIC HISTORY OF SOME METAMORPHIC ROCKS FROM SOUTHERN SINAI, EGYPT

ABDEL-AAL ABDEL-KARIM [1], ZUARD PUSKÁS [2], MELINDA JÁNOSI [2]

[1] Geology Department, Faculty of Science, Zagazig University, Egypt.
[2] Department of Petrology and Geochemistry, Eötvös Loránd University, Hungary
e-mail: abdelaalabdelkarim@hotmail.com

ABSTRACT

The Baba schists and gneisses, in the extremely northwestern part of the metamorphic belt of Sinai, have been discussed in terms of the mode of occurrence, evolution of mineral chemistry, major, trace and rare earth elements (REE) and age dating. They exhibit a trondhjemitic composition and comprise four metamorphic zones, namely the chlorite, biotite, almandine and cordierite zone. They are derived from pelitic + semi-pelitic rocks affected by three episodes of metamorphism. The first episode is a low-grade regional metamorphism of greenschist facies, the second episode is lower amphibolite facies metamorphism with higher temperature and similar pressure followed by the third episode of a retrograde metamorphism with decreasing temperature and pressure.

Chemically, the schists and gneisses are similar to crustal sediments and evolved intermediate igneous rocks, which are the source of these sediments. We assume that, they represent metamorphosed pelitic and intermediate volcanoclastic sediments that underwent hydrothermal alteration and were affected by metamorphic differentiation and partial melting. The schists and gneisses have REE patterns analogous to the intermediate igneous rocks of island arc. There are minor but interesting differences between schists and gneisses. The gneisses are characterized by higher contents of TiO_2, Hf, Ta, U, Zr, Nb and REE and lower contents Sc, Cr and Co relative to the schists, probably due to the influence of the accessory zircon, apatite and monazite and/or the more pronounced effects of the metamorphic differentiation on the gneisses.

K-Ar age dating of gneisses gives ages of 620 ± 24 Ma and 602 ± 23 Ma. The former age may represent the nearest estimated age for the formation of the protolith of the gneisses, meanwhile, the second one probably records the age of metamorphism. The schists yield an age of 549 ± 22 Ma, which may be represent the late retrograde metamorphism effected the schists.

Key words: gneisses, schists, Southern Sinai, mode of occurrence, geochemistry, K-Ar age dating, origin, and metamorphic evolution

INTRODUCTION

Metamorphic rocks are of limited distributed in Sinai massif and represent, together with some sediments, the oldest rocks in the Precambrian area of the district. They are believed to have formed through regional metamorphism took place about 1100-1300Ma (El-Shazly et al., 1973; Siedner et al., 1974). These rocks occur in a few exposures in Sinai. The larger exposure is the Wadi Feiran-Solaf belt (Akaad et al., 1967 a, b, 1988; El-Gaby, Ahmed, 1980) which locates only about 30 km south of the studied area.Some of the metamorphic rocks of the Wadi Baba area under study have been examined and mapped by El-Aref et al. (1988, 1989). They studied the geology geochemistry and fabric evolution of the migmatitic rocks. According to them these migmatitic rocks are formed by migmatization processes including metamorphic differentiation, limited and higher degrees of partial melting and were metamorphosed up to amphibolite facies. Only a few age dating of some schists and gneisses from the metamorphic belt of Sinai have been discussed. Elat schists yielded 807 ± 35 Ma with Sr87/ Sr86 initial ratio of 0.7030 for the biotite-muscovite chlorite-garnet schist (Halpern, Tristan, 1981) and 791 ± 48 Ma with 0.7030 initial ratio for age of sedimentation of the biotite-muscovite-amphibole schist (Bielski, 1982). The latter author reported that the Feiran and Fjord gneisses have age of 641-656 Ma with initial Strontium ratio of 0.7073-0.7043. Stern and Manton (1987) reported that the Wadi Feiran paragneisses gave 632 ± 3 Ma for the U-Pb zircon age and 610 Ma ago for Rb-Sr whole rock dating. This paper discusses the petrology, mineral chemistry, geochemistry and age dating aspects to through light on the origin, the tectonic environment and the conditions that prevailed during the metamorphism of these rocks.

METHODS

Thirty nine chemical analyses of chlorite (9), muscovite (6), biotite (11), garnet (10) and cordierite (3) from the schists and gneisses of Wadi Baba area, southwest Sinai have been carried out using a computerized AMRAY-1830 IT6 electron microprobe analyzer operated at 20 KV accelerating voltage, with 1-2 nA specimen current. Ten rock samples from schists and gneisses were analyzed for major elements by standard wet chemical technique. Also, six of these samples were analyzed for the trace elements Sc, Cr, Co, Zn, Rb, Ba, Cs, Hf, Ta, Th, U, Sr, Nb, Y, Zr and rare earth elements (REE). Trace elements were determined by standard instrumental neutron activation analysis (INAA) except for Nb, Y and Zr which were measured by the optical atomic spectro-photometry method (PGS-2C Zeiss Jena) and REE in the Atomic Reactor of Technical University and Sr by atomic absorption technique (AA 474). The analyses of microprobe and major elements together with Sr, Nb, Y and Zr were carried out in the Department of Petrology and Geochemistry of Eotvos University and trace elements University, Budapest. Selected three analyses for biotite fractions separated from the studied schist and gneiss were

measured by K-Ar age dating method. The analyses were carried out in the Institute of Nuclear Research (ATOMKI) of Hungarian Academy of Science in Debrecen, Hungary.

Geological Setting

Schists and gneisses of Wadi Baba constitute an important part in the metamorphic belt of the extreme northwestern Sinai massif (Fig. 1). This belt forms isolated small bodies (up to 2 km^2) exposing in Wadis Baba, Hamata, el-Sih, Nukhul and Khaboba. Many more occurrences of the belt are certainly hidden under widely distributed thick beds of the Cambrian Ordovician sandstone (Weissbrod, 1969) and Carboniferous carbonates (EL-Aref et al., 1988). Schists and gneisses under study constitute the main rock types of Baba metamorphic belt. They form low to moderate hilly rocks, tectonically controlled, trend NNW-SSE and NW-SE direction and exhibit a pronounced banded structure. The general dip of foliation is NW-SE direction with angle dip of 120° / 30°. The studied schists and gneisses are dissected by number of pegmatite and quartz veins, which are often intercalated with the general trend of foliation. The schists and gneisses are deep green to dark grey in colour. The grain size, type of mineral assemblage and grade of metamorphism appear to be graded from schists to gneisses. These rocks are enclosed in the older granites, intruded by younger granites and cut by mafic and felsic dykes and are regionally overprinted by greenschist to lower amphibolite facies. The older granites are massive to gneissose, coarse-grained, dark grey colour and range in composition from quartz diorite to granodiorite. The younger granites are medium to coarse-grained and occasionally porphyritic, pinkish in colour and range from monzogranite to syenogranite and even alkali feldspar granite. They show irregular contact with metasedimentary country rocks. Due to the intrusion of granitic rocks, the original low-grade metasediments (chlorite schists) are subjected to contact metamorphism and subsequently transformed into medium-grade pelitic to semi-pelitic schists and gneisses.

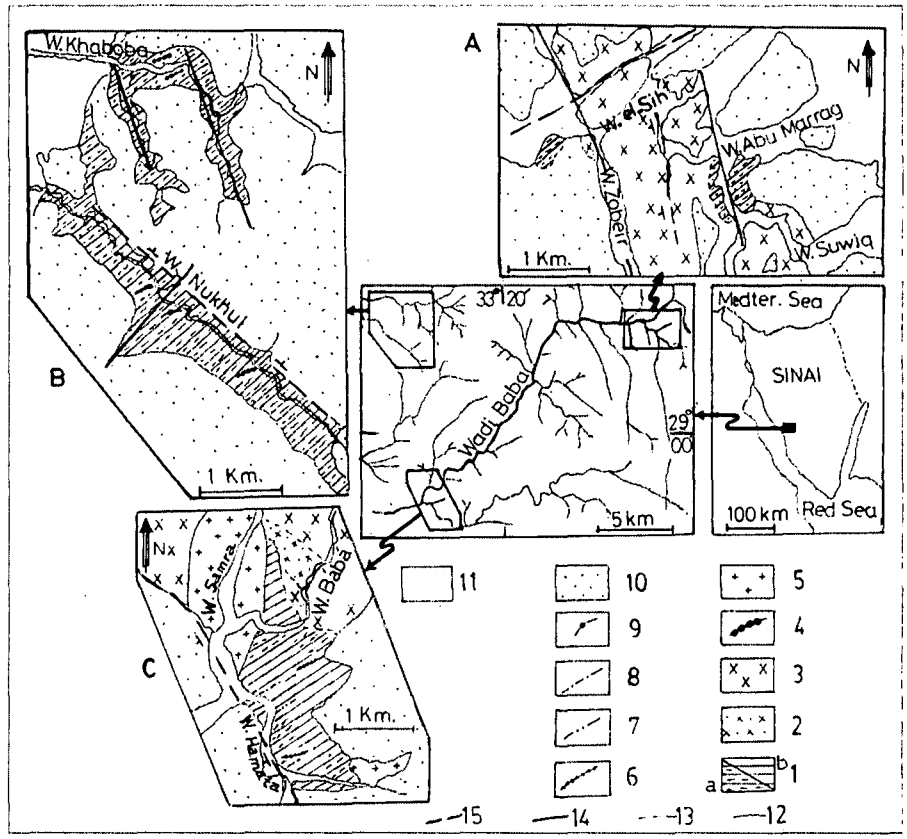

Fig. 1. Location map of the studied schists and gneisses of Wadi Baba area, SW-Sinai. A, B and C) geological maps for Wadis el-Sih, Khaboba and Nukhul and Hamata areas. Designation: 1=Metamorphic rocks, a) schists, b) gneisses; 2=Metagabbro-diorite complex; 3=Older granites; 4=mafic dykes; 5=Younger granites; 6=felsic dykes; 7=pegmatitic veins; 8=quartz veins; 9=basaltic dykes; 10=Phanerozoic sediments; 11= Wadi deposits:12= sharp contacts; 13=gradational contacts; 14=minor tectonic lines; 15=major normal faults

Table 1. The main petrographic features of the Baba schists and gneisses.

Rock name	Metamorphic texture	Mineral assemblage Essential	Accessory	Seconary
Mus-chl-gar-bio schist	porbl, lepbl.	alb, bio, qz, gt, mus.	zir, ap, tou.	chl.
Bio schist	lepbl, poikbl.	olig, bio, qz.	zir, ap.	ser, kao.
Gar-bio schist	porbl, lepbl.	olig, bio, qz, gar.	zir, ap.	chl.
Sil-gar-bio schist	poikbl, lepbl.	ab, bio, qz, gar, sil.	zir, ap, tou.	chl, ser.
Sil-cord-bio schist	lepbl, hel.	ab, bio, qz, crd, sil.	zir, ap, tou.	chl, ser.
Bio gneiss	–	olig, bio, qz, kf.	zir, ap.	ser, kao.
Cord-bio gneiss	lepbl, poikbl.	olig, bio, qz, crd, kf.	mon, ap.	ser.
Gar-cord-bio gneiss	porbl, lepbl.	olig, bio, qz, cord, gar.	zir, mon.	ser, kao.
Sil-cord-bio gneiss	lepbl, hel.	olig, bio, qz, crd, sil.	mus, zir, mon, ap.	ser.

Abbreviations – Minerals: alb=albite, and=andesine, ap=apatite, bio=biotite, chl= chlorite, cord=cordierite, gt=garnet, kao=kaolinite, kf=k-feldspar, mon=monazite, mus=muscovite, olig=oligoclase, qz=quartz, ser=sericite, sil=sillimanite, tou=tourmaline, zir=zircon. Textures: grabl=granoblastic, hel=helicitic, lepbl=lepidoblastic, poikbl=poikiloblastic, porbl=porphyroblastic

PETROGRAPHY

Microscopically, these rocks made up of plagioclase, biotite, quartz, garnet, chlorite, muscovite and cordierite ± sillimanite. The accessory phases include zircon, apatite, tourmaline and monazite. The main secondary phases comprise chlorite, sericite and kaolinite. The main petrographic features including the petrographic varieties, textures and mineral assemblages are summarized in Table 1. Moreover, the modal composition of the studied rocks is listed in Table 2. The present schists and gneisses have been affected by three main phases of deformations. D_1 is represented by the main foliation of the rocks (S_1), mineral lineation and segregation of quartz streaks parallel to the foliation. D_2 resulted in deformation of S_2 and the formation of

Table 2. Results of modal composition of Baba schists and gneisses

Rock name, no.		pla	bi	q	mu	ga	cr	si	k	ch	Acc	Su
Schists.	257	52	10	2	6	5	-	2	-	3	-	100
	210	53	15	2	-	3	-	-	-	3	1	100
	183	50	9	2	2	4	-	5	-	4	-	100
	197	54	15	2	-	-	-	1	-	3	1	100
	280	49	4	2	-	4	5	2	-	8	1	100
Gneisses:	36	49	23	2	2	-	-	-	1	1	1	100
	11	29	35	1	-	-	20	-	1	-	1	100
	265	49	15	1	-	4	12	-	1	-	1	100
	13	48	12	1	-	-	17	4	-	2	1	100

discordant with Se (Fig. 2B). The foliation of the matrix often warps around the garnet porphyroblast. Also, there is a marked cracking or straining in the porphyroblast which is angularly discordant with S_e.c) Syn-tectonic porphyroblast growth in which a classic "snowball garnet" with about 360° rotation during growth (Fig. 2C).This consists of a spiral pattern inclusions within the porphyroblast being rolled by shear along the schistosity plane as it grew.

MINERAL CHEMISTRY

Microprobe data of chlorite, muscovite, biotite, garnet and cordierite occurring in schists and gneisses together with their structural formulae are given in Table 3. The

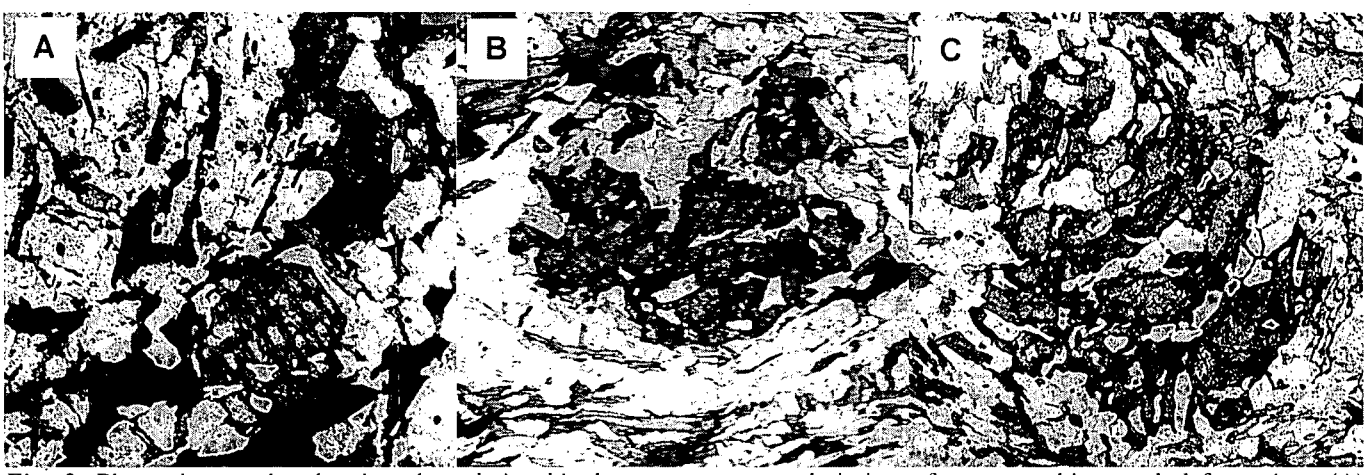

Fig. 2. Photomicrographs showing the relationship between garnet and timing of metamorphism and deformation: *(A)* nucleation and development of idiomorphic garnet in a fine-grained schist, *(B)* pre-tectonic porphyroblast growth in which the Si and cracking of garnet are discordant with Se, *(C)* syn-tectonic porphyroblast growth in which classic "snowball garnet" is rotated more than 180° during growth

second mineral lineation. D_3 is represented by the formation of S_3 and development of minor folds, kinks and granodioritic veins. The relationships between metamorphic textures and the timing of metamorphism and deformation reveal three stages of evolution relative to the pattern of inclusions in garnet porphyroblasts (S_i) and the dominant foliation in the rest rocks (S_e). These features appear in Fig. 2 and comprise the following: a) Nucleation of garnet in fine-grained schist (Fig. 2A) by diffusion of material towards a newly formed nucleus until the rock has begun to equilibrate with it.b) Pre-tectonic porphyroblast growth in which the the internal fabric (S_i) is likely to be

Table 3. Results of microprobe analysis of selected minerals, Baba schists and gneisses

Chlorites									
	Schist						Gneiss		
	257	257	257	183	183	183	36	36	36
	F11	F12	F13	H11	H12	H13	M11	M12	M13
	core		rim	core		rim	core		rim
SiO_2	26.09	26.08	26.16	22.55	25.92	25.6	27.89	27.47	26.90
Al_2O	22.36	22.49	22.85	22.8	23.12	22.73	19.52	19.41	19.94
FeO_t	22.5	22.5	23.02	23.70	23.64	23.7	26.74	26.93	28.26
MgO	17.25	17.23	17.18	15.85	15.72	15.66	14.23	14.32	13.66
Sum	88.20	88.3	89.21	87.90	88.4	87.69	88.38	88.13	88.76
Cation numbers based on 28 Oxygenes									
Si	5.364	5.355	5.326	2.307	5.342	5.329	5.836	5.780	5.664
Al	5.419	5.444	5.484	5.583	5.617	5.578	4.815	4.815	4.394
Fe	3.860	3.855	3.911	4.107	4.065	4.117	4.669	4.728	4.965
Mg	5.283	5.270	5.211	4.904	4.826	4.857	4.436	4.489	4.284
Xmg	0.58	0.58	0.57	0.54	0.54	0.54	0.49	0.49	0.4

analyses minerals exhibit major compositional variations. Graphical representation of these minerals on the AFM diagram (based on Winkler, 1976) is shown in Fig. 3. In this figure, the data points of the studied minerals plot in or near fields of the same mineral assemblage which characterize the pelitic rocks. Chlorites: 3 chlorite grains, 2 from schist and 1 from gneiss were analysed (Table 3).The analysed chlorites were plotted on the $Fe_t/(Fe_t+Mg)$ ratio versus Si classification diagram of Hey (1954) (Fig. 4). In this figure the chlorites of the schist fall in the ripidolite field while that from gneiss fall in the pycnochlorite field. The analysed chlorites from gneiss are enriched in Si compared with that from schist. Nevertheless, the Mg decreases and the Si increases from schist to gneiss with progressive

Table 3 continued

Muscovites							Cordierrites			
	Schist			Gneiss				Schist		Gneiss
	257 G11 core	257 G12	257 G13 rim	36 L11 core	36 L12	36 L13 rim		280 M11 core	280 M12 rim	13 N11
SiO_2	46.37	45.66	46.92	46.23	46.70	45.82	SiO_2	47.50	47.20	46.85
Al_2O_3	33.66	34.49	34.14	34.47	.4.23	34.94	Al_2O_3	61.60	32.38	30.81
TiO_2	0.78	0.50	0.35	0.67	0.63	0.58	FeO_t	8.65	8.73	9.62
FeO_t	0.79	1.81	0.85	0.93	1.21	1.14	MnO	0.05	0.04	0.05
MgO	1.33	1.51	1.32	1.28	1.16	1.18	MgO	8.52	7.55	733
Na_2O	1.67	1.86	1.77	1.71	1.78	1.72	CaO	0.54	0.52	0.53
K_2O	9.77	9.34	0.11	9.22	9.27	9.55	Na_2O	0.05	0.55	0.59
Sum	94.30	98.17	95.46	94.51	94.98	94.64	K_2O	0.45	0.48	0.49
Cation numbers based on 22 Oxygenes							Sum	97.82	97.45	96.27
Si	6.240	6.104	6.241	6.178	6.218	6.120	Cation numbers based on 18 Oxygenes			
Al_{IV}	1.760	1.896	1.759	1.822	1.782	1.880	Si	4.930	4.680	4.520
Z	8.000	8.000	8.000	8.000	8.000	8.000	Al	3.681	3.794	3.580
Al_{VI}	3.578	3.538	3.593	3.607	3.589	3.620	Fe_t	0.847	0.872	0.993
Ti	0.079	0.050	0.035	0.067	0.063	0.058	Mn	0.004	0.003	0.004
Fe	0.092	0.202	0.094	0.104	0.135	0.127	Mg	1.550	1.580	1.482
Mg	0.236	0.301	0.252	0.225	0.230	0.232	Ca	0.103	0.102	0.182
X	3.985	4.091	3.974	4.003	4.017	4.017	Na	0.050	0.060	0.065
Na	0.436	0.482	0.456	0.443	0.459	0.455	K	0.060	0.067	0.092
K	1.577	1.593	1.615	1.572	1.574	1.608	Xmg	0.66	0.61	0.60
Y	2.013	2.075	2.061	2.015	2.021	2.063				
Xmg	0.75	0.68	0.73	0.68	0.63	0.65				

Biotites											
	Schist						Gneiss				
	257 D11 core	257 D12	257 D13 rim	257 E11 core	257 E12	257 E13 rim	36 C11 core	36 C12	36 C13	36 C14	36 C15 rim
SiO_2	34.81	35.28	35.36	36.03	36.05	35.80	35.79	35.45	35.23	34.47	34.94
Al_2O_3	18.89	18.87	19.09	18.70	18.39	18.56	18.26	18.99	18.66	18.76	18.34
TiO_2	2.26	2.28	2.27	3.04	3.03	3.00	2.59	3.09	2.90	2.38	3.20
FeO_t	20.02	20.32	20.81	18.45	18.56	19.14	20.29	20.89	20.80	20.54	20.66
MgO	9.42	9.64	9.93	10.72	10.47	10.74	8.74	8.35	9.09	10.55	8.98
K_2O	9.15	9.08	9.19	8.82	9.03	8.54	8.83	8.77	8.70	8.26	8.95
Sum	94.55	95.47	93.65	95.76	95.53	95.78	94.51	95.54	94.38	94.96	95.07
Cation numbers based on 22 Oxygenes											
Si	5.319	5.336	5.297	5.372	5.399	5.348	5.454	5.354	5.366	5.318	5.322
Al_{IV}	2.681	2.664	2.703	2.628	2.601	2.652	2.546	2.646	2.634	2.682	2.678
Z	8.000	8.000	8.000	8.000	8.000	8.000	8.000	8.000	8.000	8.000	8.000
Al_{VI}	0.721	0.700	0.669	0.658	0.645	0.616	0.734	0.734	0.716	0.712	0.614
Ti	0.260	0.259	0.256	0.341	0.341	0.337	0.397	0.351	0.332	0.285	0.366
Fe	2.134	2.150	2.167	1.920	1.942	1.999	2.167	2.198	2.102	2.3034	2.191
Mg	2.145	2.173	2.217	2.382	2.337	2.392	1.985	1.880	2.064	2.314	2.039
Y	5.260	5.282	5.309	5.301	5.365	5.344	5.293	5.153	5.204	5.335	5.210
K	1.783	1.752	1.756	1.677	1.725	1.628	1.717	1.690	1.690	1.646	1.739
X	1.783	1.752	1.756	1.677	1.725	1.628	1.717	1.690	1.690	1.646	1.739
Xmg	0.50	0.50	0.51	0.55	0.55	0.55	0.48	0.42	0.50	0.50	0.48

Table 3 continued

Garnets										
	Schist					Gneiss				
	257 B11 core	257 B12	257 B13	257 B14	257 B15 rim	265 A11 core	265 A12	265 A13	265 A14	265 A15 rim
SiO_2	36.17	36.29	36.06	35.63	36.11	36.00	36.00	36.12	36.27	36.30
Al_2O_3	19.86	20.04	19.89	20.08	20.11	19.87	19.82	20.04	20.35	20.11
CaO	2.38	2.34	2.84	2.66	2.74	2.79	2.72	2.79	2.29	2.89
MnO	2.85	2.67	1.81	1.60	1.90	3.88	3.72	3.89	3.91	3.88
MgO	3.39	3.25	2.88	2.91	2.91	3.04	2.98	2.71	3.29	3.13
FeO_t	34.94	35.19	36.36	36.69	36.75	33.44	33.76	33.58	34.33	33.77
Sum	99.59	99.75	99.89	99.57	99.99	99.02	99.00	99.13	99.99	99.99
Cation numbers based on 22 Oxygenes										
Si	2.959	2.962	2.953	2.929	2.940	2.961	2.963	2.967	2.943	2.954
Al_{IV}	0.041	0.038	0.047	0.071	0.060	0.039	0.037	0.033	0.057	0.046
Z	3.000	3.000	3.000	3.000	3.000	3.000	3.000	3.000	3.000	3.000
Al_{VI}	1.864	1.880	1.862	1.864	1.860	1.877	1.886	1.897	1.879	1.873
Fe^{3+}	0.136	0.120	0.138	0.136	0.140	0.123	0.114	0.103	0.121	0.127
Y	2.000	2.000	2.000	2.000	2.000	2.000	2.000	2.000	2.000	2.000
Fe^{2+}	2.243	2.280	2.330	2.321	2.322	2.175	2.202	2.222	2.181	2.158
Mn	0.197	0.184	0.125	0.111	0.131	0.270	0.259	0.271	0.269	0.267
Mg	0.413	0.395	0.351	0.357	0.353	0.373	0.366	0.332	0.398	0.380
Ca	0.209	0.205	0.249	0.234	0.239	0.246	0.240	0.245	0.199	0.252
X	3.062	3.064	3.055	3.023	3.045	3.064	3.067	3.070	3.056	3.057
Xmg	0.15	0.14	0.12	0.13	0.12	0.14	0.14	0.13	0.15	0.14
End members										
Alm.	73.2	73.1	76.1	74.4	75.9	71.0	71.0	72.0	71.4	70.5
Pyr.	13.3	13.1	11.4	10.0	11.5	12.1	12.0	11.1	13.0	12.3
Ynd.	6.7	7.0	6.9	6.5	7.0	6.2	6.3	5.1	6.0	6.2
Spess.	6.5	6.0	4.0	3.1	4.1	8.7	8.6	9.0	8.6	8.7
Gros.	0.2	0.8	1.6	2.0	1.4	2.0	2.0	2.8	1.0	2.2

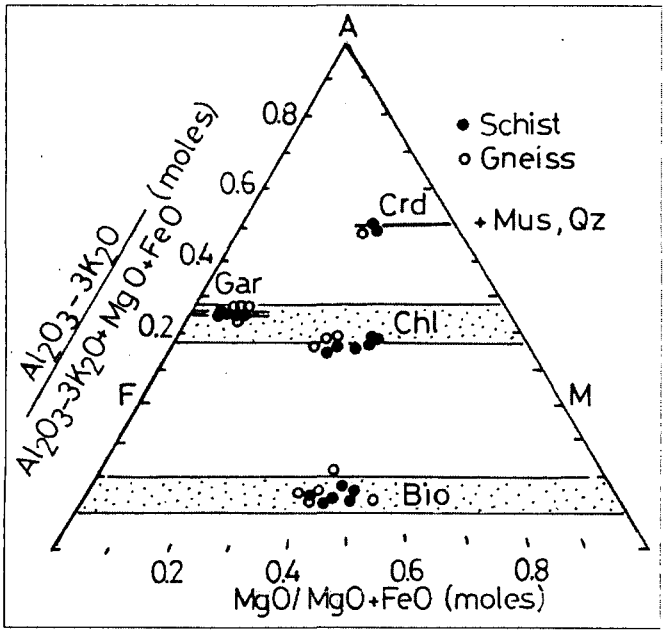

Fig. 3. Graphical representation of the analysed chlorites, biotites, garnets and cordierites into the AFM diagram (Based on Winkler, 1976). A= Al2O3-3K2O/(Al2O3-3K2O+FeO+MgO) (moles), M= MgO/(MgO+FeO) (Moles)

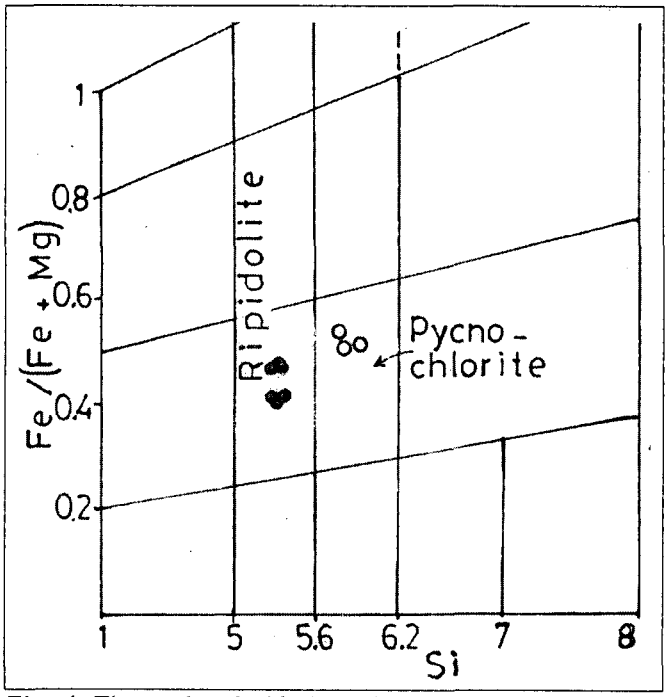

Fig. 4. The analysed chlorites plotted into Fe/(Fe+Mg)-Si classification diagram (after Hey, 1954)

metamorphism. Fet increases and Mg decreases from core to rim of the grain. Moreover, the rim of chlorite grain in gneiss is richer in Fet and poorer in Mg compared with that of schist showing evolutionary trend with the prograde metamorphism. Hyndman (1985) suggested that the composition of chlorites range from Fe-rich in chlorite zone to Mg-rich in garnet&staurolite zone [i.e. Fe_t /(Fe_t +Mg) ratio=0.5-0.8]. The analysed chlorites are Mg-Fe chlorite series and range from 0.55-0.67 with an average of 0.6, indicating their similarity with that formed in the chlorite zone. Muscovites are plotted on classification diagram of Harrison (1990), (Fig. 5A). In this figure the analysed samples from both schist and gneiss fall near the muscovite end member. Miyashiro (1973) classified the zones of muscovites into chlorite, biotite and almandine and stuarolite and sillimanite zones based on Al_2O_3 and FeO_t contents. The present muscovite plots in the field of the muscovite co-existing with the chlorite, biotite and almandine zone (Fig. 5B).

The studied muscovites have higher Si and lower Al and Na suggesting their occurrence in the chlorite zone. Lambert (1959) mentioned that the muscovite of the chlorite zone have higher Si and Fet and lower Al and Na contents than those of the biotite or garnet zone. Biotites: the investigated biotite include 2 grains from schists and 1 from gneiss (Table 3). The composition of biotites from the studied schists and gneisses are shown in Fig. 6 in terms of Al, Mg and Fe (after Nemec, 1972). This figure indicates that the analysed biotites fall on siderophyllite-eastonite line showing an equal values of these terms. Several studies have concluded that the Ti and Mg contents of biotite increase with increasing grade of metamorphism (Guidotti, 1984). The analysed biotitea are characterized by increase of Mg (from 2.15 and 2.38 in core to 2.22 and 2.4 in rim of the schists and from 1.99 in core to 2.04 in rim of the gneisses) with increasing grade, suggesting an increase in metamorphic grade from cor to rim of biotite flakes in both schists and gneisses. This increase of Mg in biotite is equilibrated partially with the decrease of Mg in the chlorite. Garnets were represented by 1 grain from each of schist and gneiss. (Table 3). The composition of garnets are shown in Fig. 7, in terms of pyrope, andradite+ grossular and almandine end-members. In this figure the analysed garnets are almandine showing their pronounced Fe_2+ contents (Alm=70-76 %). The analysed garnets are normally zoned particularly in the schists: the MnO contents decrease from 2.85 in the core to 1.90 in the rim while FeOt increase from 34.94 to 36.75 in the same direction. The contents of FeO_t , CaO and Al_2O_3 increase while MnO and MgO decrease from core to rim of the present almandine crystals from schists and gneisses. This variation in Fe, Ca, Mn, Mg and Al could be interpreted in terms of initial bedding modified by subsequent rotation during deformation (Thompson et al., 1977) or due to the equilibrium of reactions between the garnets and the matrix. Moreover, the analysed almandines are analogous to that from metapelites of the high temperature part of the almandine zone of the Barrovian region which commonly contain about 0.6% MnO, 28% FeO_t, 3-4% MgO and several percent CaO (Atherton, 1968). The isograde of this almandine probably closes to the epidote-amphibolite facies.Cordierites are mostly classified into magnesian- or iron cordierite. The analysed cordierites consist mainly of SiO_2 and Al_2O_3 and equal amounts of FeO

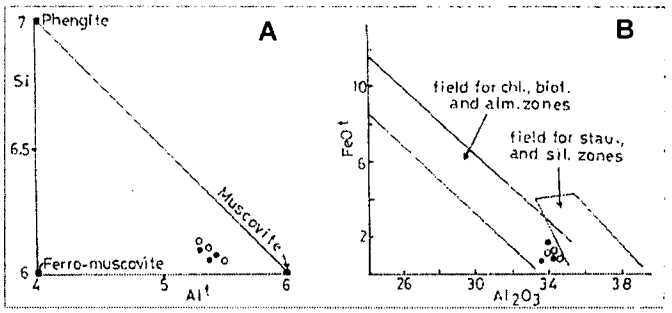

Fig. 5. The analysed muscovites plotted into: *(A)* Si-Alt classification diagram (after Harrison, 1990) and *(B)* FeOt-Al_2O_3 diagram (after Miyashiro, 1973)

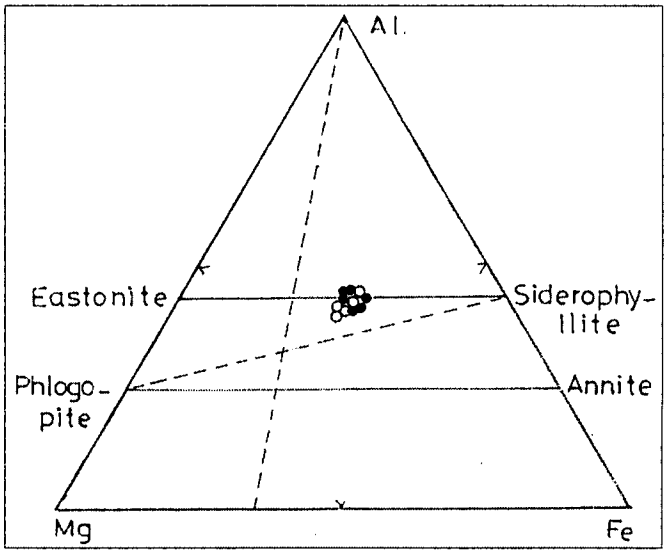

Fig. 6. The analysed biotites plotted into Al-Mg-Fe classification diagram (after Nemec, 1972)

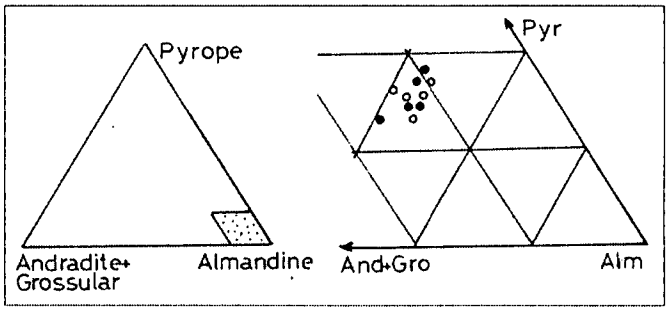

Fig. 7. The analysed garnets plotted into pyrope-andradite +Grossular-almandine diagram

and MgO contents. Consequently, they are analogous to the Fe-Mg cordierite.

The analysed minerals are characterized by XMg cord (0.66-0.60, with average of 0.63) > chl (0.49-0.58, average 0.53) > biot (0.42-0.55, average 0.50) > gar (0.12-0.15, average 0.14). This results are consistent the data given by Yardley (1989) who reported that the XMg cord > XMg chl > XMg biot > XMg gar in the pelitic rocks.

THERMOBAROMETRY

The following series of metamorphic zones have been delineated on the basis of mineral changes in response to P-T conditions. The pelitic chlorite in low grade metamorphic assemblage has crystallized at T=400 °C and PH_2O+2 kb. (Winkler, 1976). Chlorite become unstable at T=505-555 °C

and P=0.5-4 kb (Velde, 1964). Biotite breaks down at temperatures between 400 °C and 800 °C at 2 kb depending on the oxygen fugacity. The studied biotite has Mg/(Mg+Fe) ratio of about 0.5. This ratio is similar to that given by Wones, Eugster (1965) (i.e. 0.45) for the biotite stable up to 800 °C. This indicates that the stability of present biotite is less than 800 °C. The stability of almandine under low oxygen fugacity is expanded greatly with increasing pressure: at 2 kb in the presence of H_2O it is stable up to 350 °C and this range increases to nearly 850 °C at 20 kb in the absence of H_2O (Hsu, 1968). Nevertheless, the stability of the analysed almandine is less than 850 °C. Pure Mg-cordierite has its lower stability limit around 500 °C at 2 kb. The upper stability limit of this cordierite is about 7 kb. In dry systems. Fe-cordierite is similar to its Mg-member in respect to the lower temperature limit. The upper stability limit of Fe-cordierite is about 3.5 kb at 700 °C (Richardson, 1968). Accordingly the stability of present Mg-Fe cordierite is more than 500 °C.

GEOCHEMISTRY

The applicability of the chemical data (Table 4, 5), in illustration of metamorphic evolution, depends to a large extent on the amount of chemical alteration, mobility and

Table 4. Results of the chemical composition of Baba schists and gneisses

	Schists						Gneisses					
	257	280	183	210	142	Av.5	13	36	15	11	266	Av.5
SiO_2	69.23	65.96	64.05	63.12	61.85	64.8	65.70	65.68	63.20	62.11	62.02	63.7
TiO_2	1.06	0.89	1.35	0.71	1.13	1.0	1.05	0.60	1.44	1.65	1.03	1.2
Al_2O_3	13.53	14.63	14.40	14.66	15.24	14.5	14.76	14.54	15.80	15.59	15.71	15.3
Fe_2O_3	0.18	0.28	<0.10	3.26	0.84	0.9	0.85	2.16	0.15	<0.10	0.37	0.7
FeO	4.36	4.55	6.48	2.95	6.05	4.9	5.20	3.75	6.70	6.80	5.73	5.6
MnO	0.06	0.08	0.07	0.07	0.08	0.7	0.07	0.07	0.06	0.06	0.05	0.6
CaO	1.45	1.12	1.30	2.53	1.94	1.7	1.73	2.44	1.52	1.88	1.78	13.9
MgO	2.87	3.62	3.53	3.42	2.98	3.3	2.84	2.99	3.60	3.65	3.45	3.3
Na_2O	2.82	3.03	3.37	3.77	2373	3.1	3.05	3.30	2.99	2.79	2.87	3.0
K_2O	1.97	2.07	1.82	2.23	1.87	2.0	1.93	1.30	2.11	2.60	2.55	2.1
H_2O^-	0.45	0.50	0.42	0.68	0.55	0.5	0.48	0.43	0.40	0.34	0.41	0.4
P_2O_5	0.10	0.12	0.13	0.20	0.09	0.1	0.17	0.18	0.21	0.05	0.07	0.1
LOI	1.82	2.72	2.50	2.30	2.84	2.7	1.64	2.53	1.70	1.96	2.64	2.7
Sum	99.90	99.43	99.52	99.99	98.19	99.2	99.47	99.97	99.88	99.58	98.68	99.6
Sc	17.5	16.3	18.2	-	-	17.3	-	15.0	18.8	19.7	-	17.8
Cr	155.0	210.0	133.0	-	-	166.0	-	183.0	122.0	125.0	-	143.0
Co	18.3	16.5	18.7	-	-	17.8	-	19.2	19.8	19.5	-	19.5
Zn	205.0	101.0	235.0	-	-	180.0	-	208.0	243.0	230.0	-	2270
Rb	102.0	n.d.	134.0	-	-	118.0	-	115.0	153.0	140.0	-	136.0
Ba	570.0	800.30	433.0	-	-	681.0	-	595.0	390.0	380.0	-	455.0
Cs	3.2	n.d.	3.3	-	-	3.2	-	3.4	3.8	3.5	-	3.6
Hf	5.4	4.9	6.4	-	-	5.6	-	8.8	8.2	7.3	-	8.1
Ta	0.8	0.9	0.8	-	-	0.8	-	0.9	1.1	0.9	-	1.0
Th	8.3	5.2	9.3	-	-	7.3	-	7.3	9.8	9.7	-	8.9
U	2.4	1.9	2.5	-	-	2.3	-	2.1	2.9	2.8	-	2.6
Sr	210.0	232.0	202.0	-	-	215.0		203.0	161.0	166.0	-	177.0
Nb	10.0	13.0	11.0	-	-	11.0		12.6	17.0	15.0	-	14.9
Y	22.0	21.0	24.0	-	-	2.2	-	30.0	29.0	27.0	-	28.7
Zr	134.0	131.0	138.0	-	-	134.0	-	155.0	153.0	149.0	-	152.0

257: Mus-chl-gar-bio schist. 13: Sil-cord-bio gneiss. 280: bio schist. 36: Bio gneiss. 183: Sil-gar-bio schist. 15 and 11: Cord-bio gneiss. 210:Gar-bio schist. 266: Gar-cord-bio gneiss. 142: Sil-cord-bio schist. n.d.: not detected. -: not analyzed.

Table 5. Rare earth elements (REE) concentations of Baba schistsand gneisses compared with that of the crust and North American Shales Composite (NASC)

	Schists				Gneisses				I.	II.	III.
	257	280	183	Av.3	36	15	11	Av.3			
La	27.6	22.5	29.3	26.4	39.0	33.1	32.5	34.9	31.6	30.0	32.0
Ce	55.0	47.0	53.7	53.7	70.0	66.0	64.0	66.7	60.2	60.0	73.0
Nd	23.0	22.0	22.3	22.3	22.0	22.5	22.0	22.2	22.3	28.0	33.0
Sm	5.7	5.3	5.6	5.6	6.8	6.4	6.1	6.4	6.0	6.0	5.7
Eu	1.3	1.2	1.2	1.2	1.4	1..8	1.5	1.6	1.4	1.2	1.2
Tb	<1.0	<1.0	1.1	1.1	1.5	1.4	1.2	1.4	1.3	0.9	0.9
Yb	4.4	4.3	4.5	4.5	4.9	5.4	5.1	5.1	4.8	3:0	3.1
Lu	0.7	0.7	0.7	0.7	0.9	1.6	1.4	1.3	1.0	0.5	0.5

I: Average of Baba schists and gneisses. II: Average of continental crust (Taylor, 1964) III: Average of NASC (Haskin et al., 1968).

migration of the elements that occurred during metamorphism. However, the literature shows conflicting opinions regarding direction and magnitude of alteration (Humphris, 1984). The major elements chemistry are considered to suffer more changes during metamorphism. However, the studied rocks are of relatively homogeneous in their chemical composition probably due to the interlayering habit of the schists and gneisses in the field.. This is reflected for example in the narrow range of their content of SiO_2 (61.8 69.2 wt %), Al_2O_3 (13.5-15.8 wt %), FeO (4.5-6.9 wt %) and MgO (2.8-3.6 wt %) as well as the cluster of the data points on the diagrams. On the AFM projection (Fig. 8A) which shows the relationships between the mineral compositions and assemblages, all the analyses cluster on the field of chlorite-cordierite-biotite-garnet. Also on the A*KF diagram (Fig. 8B) the analyses plot on the field of muscovite-cordierite-garnet-biotite. Consequently, they exhibit a greenschist to lower amphibolite facies. TiO_2 contents are moderate (0.6-1.7 wt %). Values of LOI (loss on ignition) are above 2.5 wt % which is due to several modal percent retrograde chlorite. Also, these rocks are characterized by dominance of soda over potash, high aluminum to alkali ratios and high calcium and magnesium contents (Table 4) suggesting that they were probably derived from pelitic sediments. All these chemical feature similarities indicate that the schists and gneisses are comparable and genetically related and their metamorphic evolution is intrinsic to individual samples since they occur as interlayering beds in the field. However, there are minor differences between them. The schists have mildly higher SiO_2 and lower TiO_2 and CaO contents compared with the gneisses. The Niggli al-alk versus c diagram is used to distinguish between igneous and sedimentary rocks. On this diagram (Fig. 9A) the present analyses plot in the field of sedimentary rocks (shale). Moreover, on the (al+fm) (c+alk) versus si diagram (Fig. 9B), these rocks fall in the field of the argillaceous sediments. The HFS (high-field strength) elements (particularly the REE) are mostly considered to behave relatively immobile during metamorphic

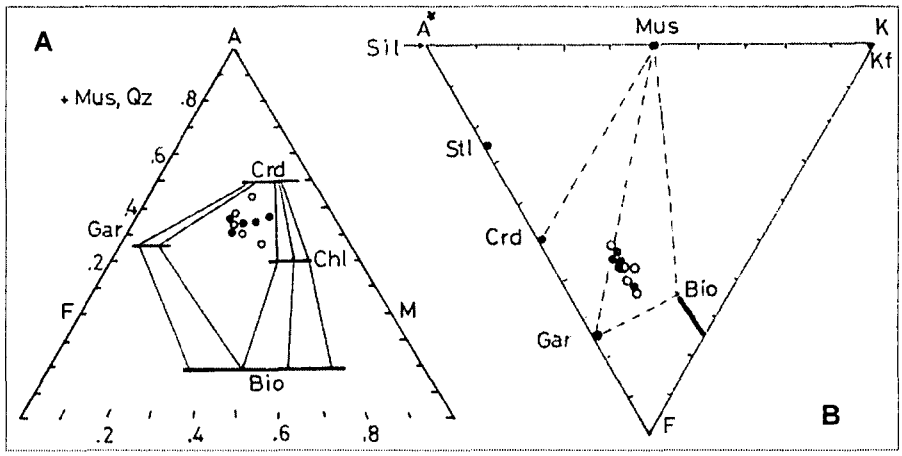

Fig. 8. The Baba schists and gneisses plotted into the combined *(A)* AFM and *(B)* A*KF projections. A*=Al2O3-CaO-Na2O+3.33P2O5, F=FeO+MgO+TiO2, K=KAlO2

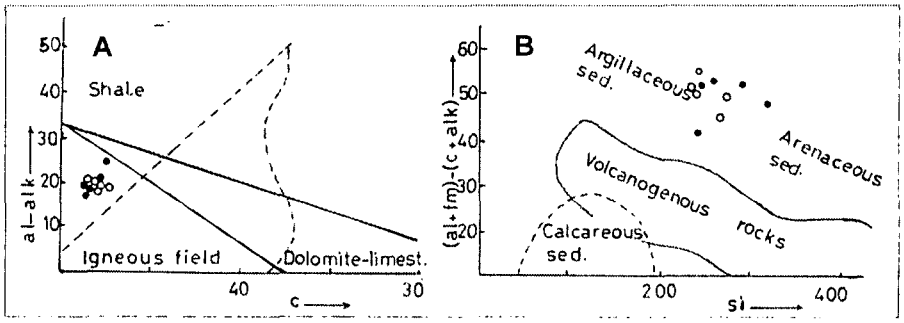

Fig. 8. The Baba schists and gneisses plotted into: *(A)* Niggli al-alk versus c diagram (after Evans and Leake, 1960) and *(B)* Niggli (al+fm)- (c+alk) versus si diagram (after Holdhus, 1971)

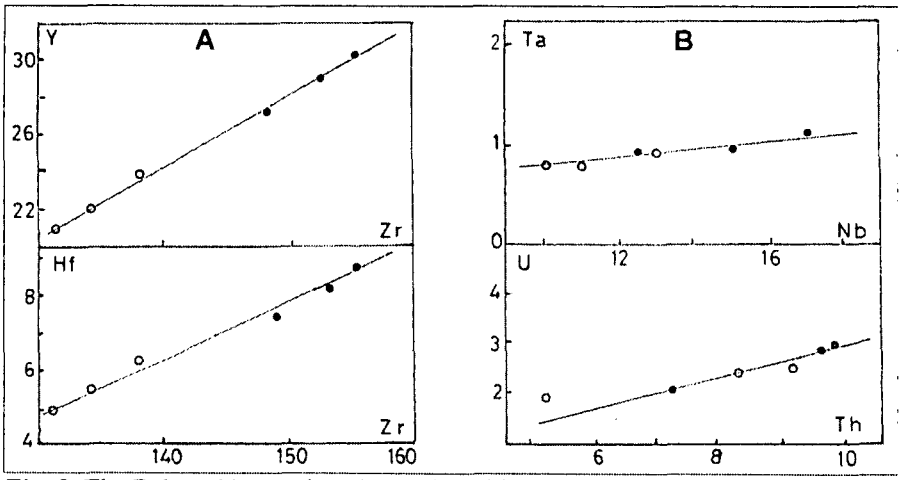

Fig. 9. The Baba schists and gneisses plotted into: *(A)* Zr vs Y and Hf and *(B)* Th vs Na and U vs Th

processes. The concentration of the trace elements in the studied schists and gneisses are mostly similar indicating their genetic relation (Tables 4, 5). However, there are minor but interesting dissimilarities between them. Yttrium concentration ranges from 21 to 30 ppm, and correlates well with the heavy REE (Tb, Yb and Lu, Table 5). Concentrations of Zr have a clear positive correlation with Y (Fig. 10A). Also, Zr correlates well with Hf and has mean Zr/Hf ratio (about 20) which is lower than the the average crustal value of about 33. Nb and Ta exhibit a good positive correlation. The mean Nb/Ta ratio in the schists and gneisses (about 15, Fig. 10B) is higher than the crustal average of about 11 (Taylor, Mclennan, 1985). Higher contents of Cr and lower Co are recorded in the schists compared with

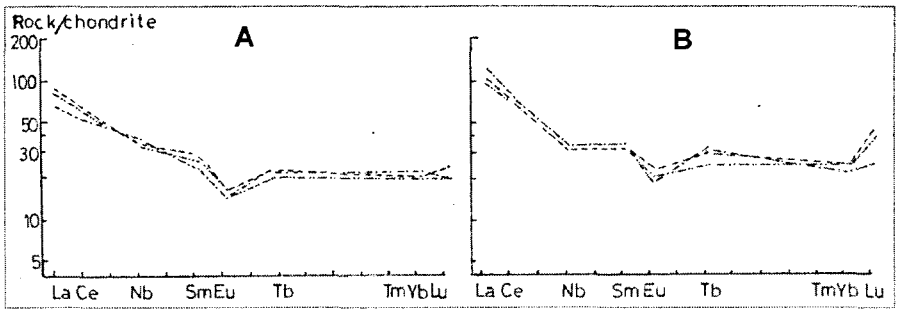

Fig. 11. Chondrite-normalized REE patterns of the studied: *(A)* schists *(B)* gneisses. The normalizing values after Wakita et al. (1971)

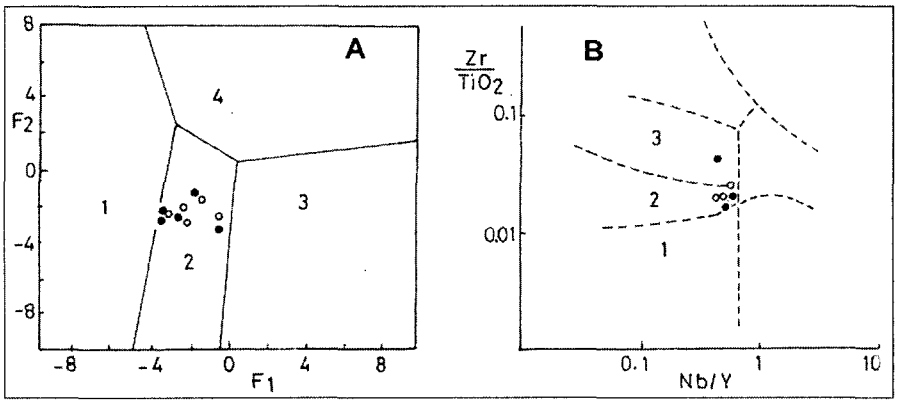

Fig. 12. The studied schists and gneisses plotted into: *(A)* F1-F2 diagram (after Roser and Korsch, 1988). Fields show provenances of 1=mafic igneous, 2=intermediate igneous, 3=felsic igneous rocks and 4=quartoze sedimentary rocks and *(B)* Zr/TiO2 vs Nb/Y diagram (after Winchester and Floyed (1977). Fields: 1=basalt, 2=andesite, 3=dacite-rhyodacite

Table 6. K-Ar age dating of the biotite fraction from Baba schists and gneisses

Sample name	locality	No.	K(%)	^{40}Ar rad. (ccSTP/g)	40AR rad. (%)	Age (Ma)
Cord-bio gneiss	W.Hamata	11	1.034	2.9688-5	75.8	620±24
Bio gneiss	W.el-Sih	36	5.416	1.5024-4	84.0	602±23
Gar-bio schist	W. Baba	60	5.147	1.2827-4	94.7	549±21

gneisses. Moreover, there are no significant correlations among these elements (Sc, Cr and Co), nor do they correlate well with FeOt. Concentrations of Rb is high, whereas Rb and Cs are relatively low in both schists and gneisses. Rb correlates positively with K and has an average K/Rb ratio (130) which is signficantly lower than the crustal average of about 250 (Taylor, Mclennan, 1985). Concentrations of Th (5.2-9.8 ppm) and U (1.9-2.9 ppm) show a significant positive correlation (Fig. 10B). The average Th/U ratio (3.5 ± 1.2) in the schists and gneisses is indistinguishable from the average of crustal value of about 3.8 (Taylor, Mclennan, 1985). Moreover, the concentrations of Hf, Ta, U, Nb and Zr are high in the gneisses compared with schists.The REE data is grouped according to assemblage (Table 5) and the Chondrite- normalized REE patterns are shown in Fig. 11. Overall, the schists and gneisses have similar REE patterns with characteristic negative Eu- anomalies. However, the gneisses are characterized by higher REE abundance (21-103 times chondrites) than the schists (19-90 times), a variety of metamorphic differentiation. REE patterns (Fig. 11) show slightly anomalous kinks for heavy REE (i.e. gneisses) consistent with the fact that Tbn<Lun in several cases may be a manifestation of a zircon effect (Dymek, Smith, 1990). The influence of zircon is emphasized again by the slight enrichment of Th and U and deletion of Nd contents which reflect the lack of apatite and monazite in the studied rocks.REE patterns are characterized by fractionated light REE compared with heavy REE (Lan>Lun). The negative Eu anomalies (as well as low Ca and Sr) probably correspond to the properties inherited from the precursor. The high abundance of REE in gneisses compared with that in schists is attributed to the relative concentrations of light REE in apatite and monazite and heavy REE in zircon and garnet during metamorphism (Nesbitt, 1979). This feature can be ascribed to the changes of fluid chemistry. Therefore, compared to schists, the gneisses have more enriched and fractionated REE patterns. Intermediate igneous rocks probably represent a more appealing precursor for the studied rocks. They contain intermediate primary SiO_2 contents, intermediate values of Sc, Cr, Co; and Zr, Hf, Ta, Th, U contents and slightly enriched and fractionated REE patterns (possibly even with negative Eu anomalies). They underwent hydrothermal alteration. Fig. 12A, a discriminant plot using function 1 (F1) versus function 2 (F2), shows that the data points of the studied rocks fall within the field if intermediate igneous provenance (Roser, Korsch, 1988). Moreover, they fall within the fields of andesite and dacite on the Zr/TiO_2 versus Nb/Y diagram (Fig. 12B).

Dating

The results of K-Ar ages are given in Table 6. While only few age dating are available for the metamorphic rocks of Sinai (Bielski, 1982; Stern, Manton, 1987), there is no age dating have been carried out on the Baba schists and gneisses. The measured K-Ar ages of the separated biotites from cord-bio gneiss of Wadi Hamata (at the entrance of Wadi Baba) and bio gneiss of Wadi el-Sih, gave 620 ± 23.9 Ma and 602 ± 22.9 Ma respectively (Table 6) with average of about 611 Ma. This average is similar to the Rb-Sr whole rock age of the Feiran paragneiss (Stern, Manton, 1987). The former age (620 ± 24 Ma) probably represents the nearest estimation to the age of formation of gneisses. The second age of gneiss (602 ± 23 Ma) can be interpreted as the higher loss of argon of the biotite probably due to the more deformed state of Wadi el-Sih gneiss, the dynamothermal as well as the effect of the metamorphic processes. Alternatively, the two ages of 620 ± 24 and 602 ± 23 Ma of the gneisses are

indistinguishable within the wide error limits. The gar-bio schist of Wadi Baba yields a 549 ± 20.6 Ma age for the separated biotite. It can be argued that this lower age may result from the strong effect of the late regression on the schists.

Discussion and Conclusion

From the former field observations, petrography and mineral chemistry of this study, it likely that most of the metamorphic mineral assemblages in the rocks crystallized under the higher temperatures reached during the P-T-t cycles. Therefore it can be assumed that there are three successive episodes of metamorphism (the early two occurred during prograde while the later during the retrograde phase) as follow:

1) The first episode of metamorphism was low-grade regional metamorphism transforming the original sediments to schists with mineral assemblage (chlorite, albite, muscovite, quartz and biotite) belongs to greenschist facies.

2) The second episode is thermal metamorphism induced by granitic intrusions on the original rocks resulting into contact schists and gneisses. The mineral assemblages of this phase (plagioclase, quartz, muscovite, biotite, garnet and cordierite + sillimanite) belong to lower amphibolite facies.

3) The third episode of metamorphism is the retrograde metamorphism due to decrease in temperature and pressure. This condition is indicated by the formation of chlorite after biotite, garnet or cordierite; muscovite and sericite after sillimanite together with secondary sericite and kaolinite after plagioclase. The metamorphic evolution of the present rocks ranges from greenshist to amphibolite facies which is intrinsic to individual samples ascribed to the interlayering of the schists and gneisses in the field. During these successive episodes the rocks have been affected by three main phases of deformation and garnet evolution. In the Baba area, the source of the heat for contact metamorphism is probably due to the intrusions of granites in the middle part of the area. The temperature of the granitic magma intrusions is generally 700-800 °C (Winkler, 1976). Near the intrusions and the metamorphic rocks there is often masses of granitic gneisses which exhibited a sign of migmatization. To get an idea on the geotectonic position in which the sediments were deposited, log (K_2O/Na_2O) versus SiO_2 diagram after Roser and Korsch (1986) was used. On this diagram the studied schists and gneisses exhibit the island arc setting (Fig. 13A). A systematic relationships involving La-Sc-Th-Co-Hf have proposed by Mclennan and Taylor (1984) and Taylor and Mclennan (1985) to indicate crustal sources of Archean sediments. Fig. (13B) shows data for Baba schists and gneisses plotted on TH-Hf-Co and La-Th-Sc diagrams. On the diagrams, the data fall in the field of NASC (North American Shale Composite) of Gromet et al. (1984), even nearby the TT (Tonalite-Trondhjemite components) of the Talyor, Mclennan (1985) of the mixture band consistent with derivation from these kinds of rocks. These rocks have high contents of La, Sc and Co and low Th and Hf contents. However, the gneisses are characterized by higher contents of La and Hf and lower Th, Sc and Co compared with the schists probably due to either the influence of minor zircon and monazite or the depletion of Th during low grade metamorphism. The studied rocks have high contents of incompatible trace elements (Zr, Nb, Y, Hf, Ta, Th, U, REE). Some or all these elements can be harbored predominantly in minor mineral phases, which could be controlled either by small quantities of detrital minerals (i.e. zircon, monazite) or reflect selective cavenging by these phases during metamorphism (Dymekm, Smith, 1990). The high and variable La contents, as well as variable chondrite normalized

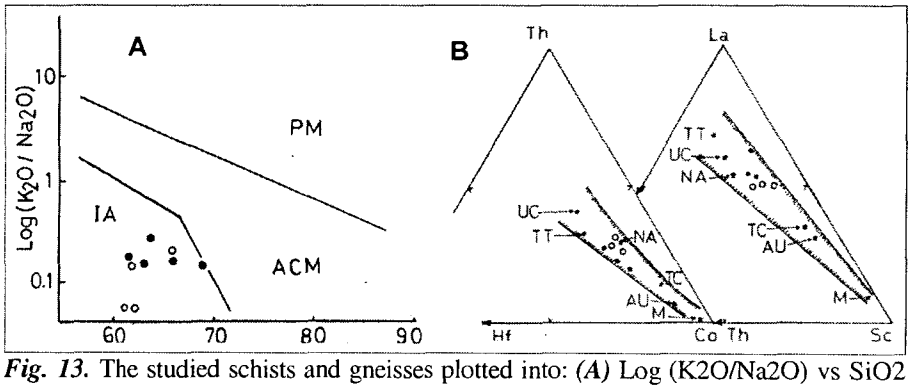

Fig. 13. The studied schists and gneisses plotted into: *(A)* Log (K2O/Na2O) vs SiO2 diagram (after Roser and Korsch, 1986). IA=island arc, ACM=active continental margin, PM=plate margin and *(B)* Th-Hf-Co and La-Th-Sc diagrams. Values of M=mafic component, TT=tonalite-trondhjemite component, AUC=Archaean upper crust, UC=upper crust and TC=total crust are from Taylor and Mclennan (1985); value of NASC=North American Shale Composite taken from Gromet et al. (1984). Stippled regions correspond to a mixing band of the composition of Archaean sediments and metasediments (after Mclennan and Taylor, 1984)

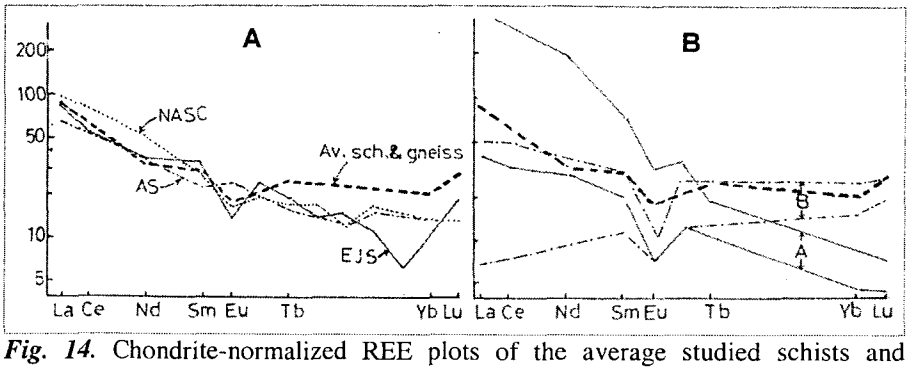

Fig. 14. Chondrite-normalized REE plots of the average studied schists and gneisses compared to: *(A)* NASC of Haskin et al. (1968), European and Japanese Shale (EJS) of Minami (1935) and Archaean Sediments (AS) of Jenner et al. (1981) and *(B)* range of intermediate igneous rocks from continental (A) and island arc (B) setting (Cullers and Graf, 1984)

(Lan/Smn) ratios, could due to either effect. Zircon, apatite and monazite have been observed in thin sections of the schists and gneisses. REE abundance and fractionations have been comparable with references REE of the crust (Taylor, 1964) and North American Shale Composite (NASC) (Haskin et al., 1968, Table 5). However, they are slightly enriched in the heavy REE abundance with respect to the references. Fig. 14A compares the average REE pattern for schists and gneisses to those of Archean sediments (Jenner et al., 1981), NASC (Haskin et al., 1968) and European and Japanese shale (EJS) (Minami, 1935). It appears that the studied rocks have a light REE and negative Eu anomaly quite similar to that from Archean sediments, NASC and EJS, but with a higher heavy REE pattern probably due to the effect of metamorphism or correspond to the properties inherited from the precursor. The high concentration of heavy REE in the examined rocks which particularly susceptible to complexion, are associated with high concentration of alkalis and volatiles (Mineyev, 1963). Furthermore, the average REE of the schists and gneisses is also partially comparable with the range of REE found in continental intermediate rocks (field A) and with the same former rocks formed in island arc (field B) after Cullers and Graf (1984) (Fig. 14B). In this figure, the average REE of the schists and gneisses mostly close to the range of island arc intermediate igneous rocks (field B). According to Cullers and Graf (op. cit.) the island arc rocks have less than 14.5-15 wt % Al2O3, nearly flat REE pattern and negative Eu anomalies, which quite similar to the studied rocks. The trace and REE of the studied schists and gneisses should be used for modeling partial melting, metamorphic differentiation and crystal fractionation processes. From the former petrological and geochemical features, it can be reasonably assumed for the formation of the schists and gneisses: formation of intermediate igneous rocks Ąć weathering, transport and deposition Ąć metamorphism (regional and contact) leading to metamorphic differentiation and possibly partial melting. In the present rocks the metamorphic differentiation can be evident by the occurrence of bands. The bands probably represent synmetamorphic dykes or veins, in some cases formed by anatexis, or developed due to preferential nucleation of phases in pre-existing structural zones (Raymond, 1995). The studied gneisses gave 620 ± 23.9-602 ± 22.9 Ma K-Ar ages with an average of 611 Ma which consistent with the result reported by Stern, Hedge (1985) and Stern, Mantin (1987). They concluded that the tectonomagmatic episode responsible for the formation of these metasedimentary rocks may have been related to the 610-630 Ma compressional events important in the evolution of the Central and Northeastern Desert of Egypt (Stern, Hedge, 1985; Stern, Mantin, 1987).

ACKNOWLEDGEMENTS

The authors are grateful to Prof. M. Okrusch, Mineralogical Institute, Wurzburg University, Germany, for the valuable discussions and critical comments of the manuscript.

REFERENCES

AKAAD, M. K., EL-GABY, S., ABBAS, A. A. (1967a): Geology and petrography of the migmatites around Feiran Oasis, Sinai. Assuit Sci. Techn. Bull., **10**, 67-87.

AKAAD, M. K., EL-GABY, S., ABBAS, A. A. (1967b): On the evolution of Feiran migmatites. J. Geol. Egypt, **11**, pp. 4958.

AKAAD, M. K., EL-GABY, S., AHMED, A. A. (1988): Feiran - Solaf district, Southwestern Sinai, Egypt. Annals Geol. Surv. Egypt, 112-132.

ATHERTON, M. P. (1968): The variation in garnet, biotite and chlorite composition in medium grade pelitic rocks from the Dalradian, Scotland, with particular reference to the zonation of garnet. Contrib. Mineral. Petrol., **18**, 347-371.

BIELSKI, M. (1982): Stages in the evolution of the Arabian-Nubian Massif in Sinai. Ph. D. Thesis, Hebrew Univ., pp. 155.

CULLER, R. L., GRAF, J. L. (1984): Rare earth elements in igneous rocks of the continental crust: Intermediate and silicic rocks-ore petrogenesis. In Henderson, P. (ed.): Rare earth element geochemistry. 275-316.

DYMEK, R. F., SMITH M. S. (1990): Geochemistry and origin of Archaean quartz-cordierite gneisses from the Godthabsfjord region, west Greenland. Contrib. Mineral. Petrol., **105**, 715-730.

EL-AREF, M. M., ABD EL WAHID, M., KABESH, M. (1988): On the geology of the basement rocks, east of Abu Zenima, West Central Sinai, Egypt. Egypt. J. Geol., **32**, 1-2, 1-25.

EL-AREF, M. M., ABD EL WAHID, M., KABESH, M. (1989):Fabric evolution and geochemical characters of the migmatites and associated gneisses of Wadi Baba and Wadi Dafari, West Central Sinai, Egypt. Egyptian Mineralogist, **1**, 27-53.

EL-GABY, S., AHMED, A. A. (1980): The Feiran-Solaf gneiss belt, SW of Sinai, Egypt. In Al-Shanti, A. M. S.(ed.): Evolution and mineralization of the Arabian-Nubian Shield. Inst. App. Geol. (Jeddah), Bull., **3**, 95-105.

EL-SHAZLY, E. M., HASHAD, A.H., SAYYAH, T. A., BASSYUNI, A. (1973): Geochronology of Abu Swayel area, South Eastern esert, Egypt. Egypt. J. Geol., **17**, 1-18.

EVANS, B. W., LEAKE, B. E. (1960): The composition and origin of the stripped amphibolites of Connemers Ireland. J. Petrology, **1**, 337-363.

GIUDOTTI, C. V. (1984): Micas in metamorphic rocks. Reviews in Min., **13**, 357-367.

GROMET, L. P., DYMEK, R. F., HASKIN, L. A., KOROTEV, R. L. (1984): The "North American shale composite". Its compilation, major and trace element characteristics. Geochim. Cosmochim. acta, **48**, 2469-24.

HALPERN, M., TRISTAN, N. (1981): Geochronology of the Arabian-Nubian Shield in southern Israel and eastern Sinai. J. Geol., **89**, 639-648.

HARRISON, T. N. (1990): Chemical variation in micas from the Cairngorm pluton, Scotland. Min. Mag., **54**, 355-366.

HASKIN, L. A., HASKIN, M. A., FREY, F. A., WILDEMAN, T. R. (1968): Relative and absolute terrestrial abundances of the rare earths. In Ahrens L. H. (ed.): Origin and distribution of the elements 1. Pergoman, Oxford. 889-911.

HENDERSON, P. (1984): Rare earth element geochemistry. Elsevier, Amsterdam, Oxford. pp. 510.

HEY, M. H. (1954): A new review of the chlorite. Min. Mag., **30**, 227.

HOLDHUS, S. (1971): Para-amphibolites from Gurskoy and Sandsoy, Sunnmor, West Norway. Norsk, Geol. Tidsskr. **51**, 231-246.

HSU, L.C. (1968): Selected phase relationship in the system Al-Mg-Fe-Si-O-H: a model for garnet equilibria. J. Petr., **9**, 40-83.

HUMPHRIS, S. E. (1984): The mobility of rare earth elements in the crust. In Henderson, P. (ed.): Rare earth element geochemistry. Elsevier-Amsterdam, Oxford. 317-342.

HYNDMAN, D. W. (1985): Petrology of igneous and metamorphic rocks, 2nd ed., McGraw-Hill, New York.

JENNER, G. A., FRYER, B. J., MCLENNAN, S. M. (1981): Geochemistry of the Archaean Yellows Knife Supergroup. Geochim. Cosmochim. Acta, **45**, 1111-1129.

LAMBERT, R. J. (1959): The mineralogy metamorphism of the Moine schists of the Morar and Knoydrat districts of Inverness-shire. Tras. Roy. Soc. Edin., **63**, 553-588.

MCLENNAN, S. M., TAYLOR, S. R. (1984): Archaean sedimentary rocks and their relation to the composition of the Archaean continental crust. In Kroner, A. et al. (eds.): Archaean geochemistry. Springer -Verlag, Berlin. 47-72.

MINAMI, E. (1935): Gehalte Seltener Erden in Europaischen and Japanischen Tonschiefern. Nachr. Ges. Wiss. Geottingen, Math.-Phys. Kl., Fachgruppe, 4, 1, 155-170.

MINEYEV, D. A. (1963): Geochemical differentiation of the rare-earths. Geochemistry (U.S.S.R.), **12**, 1129-1149.

MIYASHIRO, A. (1973): Metamorphism and metamorphic belts. John Willey & Sons, New York.

NEMEC, D. (1972): Paragenetische analyze der regional metamorphen Skarne Westmahrens. Chem. Erde, **34**, 62-84.

NESBITT, H. W. (1979): Mobility and fractionation of rare earth elements during weathering of granodiorite. Nature, **279**, 206-210.

RAYMOND, L. A. (1995): Metamorphic Petrology. Wm. C. Brown Publ., London.

RICHARDSON, S. W. (1968): Staurolite stability in a part of the system Fe-Al-Si-O-H. J. Petrol., **9**, 467-488.

ROSER, B. P, KORSCH, R. J. (1986): Determination of tectonic setting of sandstone-mudstone using SiO_2 content and K_2O/Na_2O ratio. J. Geol., **94**, 635-650.

ROSER, B. P, KORSCH, R. J. (1988): Provenance signature of sandstone-mudstone suite determined using discriminant function analysis of major-element data. Chem. Geol., **67**, 119-139.

SIEDNER, G., SHIMRON, A., PRINGLE, I. (1974): Age relations in basement rocks of the Sinai Peninsula. Int. Meet. Geochronology, Paris. 116-125.

STERN, R. J., HEDGE, C. R. (1985): Geochronological and isotopic constrains on late Precambrian crustal evolution in the Eastern Desert of Egypt. Amer. J. Sci., **285**, 97-127.

STERN, R. J., MANTON, W. I. (1987): Age of Feiran basement rocks, Sinai: Implications for late Precambrian crustal evolution in northern Afro-arabia. J. Geol. Soc. Lond., **144**, 569- 575.

TAYLOR, S. R. (1964): The abundance of chemical elements in the continental crust- a new table. Geochim. Cosmochim. Acta, **28**, 1273-1285.

TAYLOR, S. R., MCLENNAN, S. M. (1985): The continental crust, its composition and evolution. Blackwell Scientific Publications, Oxford.

THOMPSON, A. B., TRACY, R. J., LYTTLE, P. T., THOMPSON, J. B. (1977): Prograde reaction histories deduced from compositional zonation and mineral inclusions in garnet from the Gassetts schist, Vermont. Amer. J. Sci., **277**, 1152-1167.

VELDE, B. (1964): Low-grade metamorphism of micas in pelitic rocks. Carnegie Inst. Wash. Yearbook, **63**, 142-147.

WAKITA, H., REY, P., SCHMITT, R. A. (1971): Abundances of the 14 rare-earth elements and 12 other trace elements in Apollo 12 samples.: five igneous and one breccia rocks and four soils. Proc. 2nd Luner Sci. Conf., 1319-1329.

WEISSBROD, T. (1969): The Paleozoic of Israel and adjacent countries. The Paleozoic outcrops of South western Sinai and their correlations with those of Southern Israel. Geol. Surv. Israel, **48**, pp. 32.

WINCHESTER, J. A,. FLOYED, P. A. (1977): Geochemical discrimination of different magma series and their differentiation products using immobile elements. Chem Geol., **20**, 325-343.

WINKLER, H. (1976): Petrogenesis of metamorphic rocks. Springer-Verlag, New York.

WONES, D. R,. EUGSTER, H. P. (1965): Stability of biotite: experiment, theory and application. Am. Mineral., **50**, 1228-1272.

YARDLEY, B. W. D. (1989): An introduction to metamorphic petrology. Longman, London.

Received: July 11, 2002; accepted: November 23, 2002